Slater-Pauling behavior of interfacial magnetic properties of 3*d* transition metal alloy/Pt structures

Nam-Hui Kim,[1,*] Qurat-ul-ain,[2] Joonwoo Kim,[3] Eunchong Baek,[1] June-Seo Kim,[3] Hyeon-Jong Park,[4] Hiroshi Kohno,[5] Kyung-Jin Lee,[6] Sonny H. Rhim,[2,†] Hyun-Woo Lee,[7,‡] and Chun-Yeol You[1,§]

[1]*Department of Emerging Materials Science, DGIST, Daegu 42988, Korea*
[2]*Department of Physics, University of Ulsan, Ulsan 44610, Korea*
[3]*Division of Nanotechnology, DGIST, Daegu 42988, South Korea*
[4]*KU-KIST Graduate School of Converging Science and Technology, Korea University, Seoul 02841, Korea*
[5]*Department of Physics, Nagoya University, Nagoya 464-8602, Japan*
[6]*Department of Physics, Korea Advanced Institute of Science and Technology, Daejeon 34141, Korea*
[7]*Department of Physics, Pohang University of Science and Technology, Pohang 37673, Korea*

(Received 5 July 2021; revised 5 January 2022; accepted 12 January 2022; published 2 February 2022)

Ferromagnet (FM)/heavy metal (HM) bilayers are core structures for current-induced magnetization switching and chiral magnetic structure generation. Static and dynamic properties of the FM moment depend substantially on interfacial perpendicular magnetic anisotropy (iPMA) and interfacial Dzyaloshinskii-Moriya interaction (iDMI). Therefore, it is of crucial importance to control iPMA and iDMI, and to understand their underlying physics. Here we experimentally show that both iPMA and iDMI exhibit similar Slater-Pauling-like dependence on the FM variation as the saturation magnetization (M_S) does. We measure M_S, iPMA, and iDMI of the FM/HM bilayers with HM fixed to Pt and FM varied from Mn (electron number $Z = 25$) to Ni ($Z = 28$), including their alloys for fractional Z. Our result indicates that the density of states structure important for the Slater-Pauling dependence is crucial also for iPMA and iDMI. This provides a useful method to engineer chiral magnetic textures.

DOI: 10.1103/PhysRevB.105.064403

I. INTRODUCTION

Bilayer heterostructures that consist of ferromagnetic (FM) and heavy metal (HM) layers are core structures of modern spintronics. For their device applications towards magnetic memory and logic devices, their interfacial magnetic properties such as the interfacial Dzyaloshinskii-Moriya interaction (iDMI) and the interfacial perpendicular magnetic anisotropy (iPMA) play important roles [1]. The iPMA plays a central role in various spintronics devices such as spin transfer torque magnetic random-access memory (STT MRAM) [2] and spin-orbit torque memory [3], and the iDMI is an essential ingredient for static and dynamic properties of topological magnetic structures such as chiral domain wall and skyrmions [4]. Because of their large mobility, skyrmions may be controlled by a small electrical current and the emerging field of skyrmionics [5] aims to utilize skyrmions for ultradense memory and logic devices with low power consumption.

The physical origins of iDMI and iPMA are similar in the sense that they both arise from the interplay between spin-orbit coupling (SOC) and symmetry breaking at the interfaces [6]. Nevertheless there are clear differences as well; the iPMA is proportional to the square of the SOC strength [7] whereas the iDMI is linear in the SOC strength [8]. There are ongoing experimental and theoretical studies [9–13] to examine a possible correlation between the two and with other magnetic properties. To understand mechanisms of the interfacial magnetic properties, it is necessary to identify their key elements first. In the case of the iPMA, not only SOC and symmetry breaking, but also Z is important. Bruno [7] pointed out 30 years ago that the iPMA is proportional to the orbital moment, which varies with Z. Recent theoretical study [14] predict that Z is a key element for the iDMI as well. In particular, first-principles calculation [14] for monolayer 3*d* transition metals on 5*d* metals predicts that the iDMI follows Hund's first rule and depends on Z of 3*d* transition metals just as like the magnetic moment.

The relation between magnetic moments and Z has been well understood with the Slater-Pauling (SP) curve for 3*d* transition metals and their alloys [15,16]. In this class of material, the magnetic moments per atom as a function of Z show a slope of $\pm\mu_B$ (Bohr magnetic moment). In the simple rigid band model [17], the magnetic moments arise from the density of states (DOS) difference between the spin majority and minority bands. Hence in situations where one particular spin state is more than another at the Fermi energy, the SP behavior can be generic regardless of detailed band structures. On the other hand, the prediction [14] that the iDMI exhibits the similar Z dependence as the magnetic moment

*Present address: Memory Process Development Team, Semiconductor R&D Center, Samsung Electronics Ltd., Gyeonggi-Do 18448, Korea; nam-hui.kim@samsung.com
†Corresponding author: sonny@ulsan.ac.kr
‡Corresponding author: hwl@postech.ac.kr
§Corresponding author: cyyou@dgist.ac.kr

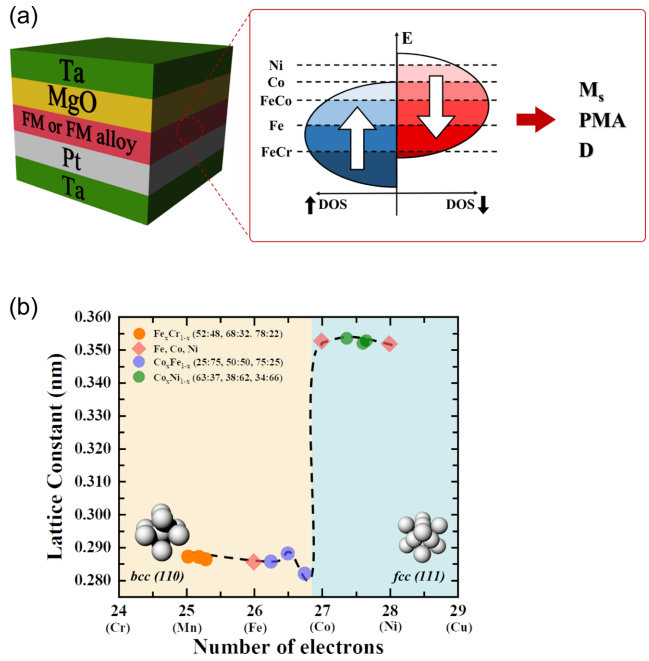

FIG. 1. (a) The schematic of sample structure based on 3*d* transition metals and their alloys. Ta(4 nm)/Pt(4 nm) are buffer layers on the SiO_2 substrate and MgO(2 nm)/Ta(2 nm) layers are deposited as capping layers. The schematic density of states (DOS) are also depicted. The saturation magnetization (M_S), interfacial perpendicular magnetic anisotropy (PMA, K_S), and interfacial Dzyaloshinskii-Moriya interaction (iDMI, D) are measured as a function of the number of electrons, or band filling. (b) The lattice parameters for all samples are determined by XRD. They clearly indicate the bcc (110) structure for FeCr, Fe, and CoFe alloys, and fcc (111) structures for the Co, Ni, and CoNi alloys.

recalls some attention as this implies the Z dependence may be related to the DOS imbalance.

We prepared a series of samples of 3*d* transition metals and their alloys on the Pt underlayer to modulate Z. Remarkably enough, the M_S, the iPMA energy density (K_S), and iDMI energy density (D) all show SP-like behavior with respect to Z: increasing to their maxima and then decreasing as Z increases. The similar Z dependence of iPMA and iDMI implies that not only SOC but also the DOS imbalance of FM layers plays an important role.

II. EXPERIMENTS

A. 3*d* transition metal alloy thin films on Pt layers

We prepared the Ta(4 nm)/Pt(4 nm)/FM or FM alloy(t nm)/MgO(2 nm)/Ta(2 nm) samples on a SiO_2 substrate by usimg a dc and rf magnetron sputtering system with a base pressure of $\sim 3 \times 10^{-8}$ Torr as shown Fig. 1(a). The thickness of the FM layer is varied from 0.6 to 1.6 nm. Here, it must be mentioned that we ignored the dead layer contribution, and all thickness in this paper means nominal thickness. We estimated the dead layer thicknesses and confirmed that they are very small and negligible. Based on the pure ferromagnet materials such as the Fe, Co, and Ni layer, we made FM with non-magnetic metal (NM) alloys structures, e.g., Fe_xCr_{1-x}, Co_xFe_{1-x}, and Co_xNi_{1-x}. For the case of Co_xFe_{1-x}, an alloy target is used with fixed compositions of $x = 0.25$, 0.5, and 0.75. On the other hand, Fe_xCr_{1-x} and Co_xNi_{1-x} were deposited by using the cosputter method dependent on deposition power.

The modulation of Z is achieved for the FM layer from 25 (Mn) to 28 (Ni). The compositions and the crystal structures of the FM alloys were verified by x-ray photoelectron spectroscopy (XPS) and x-ray diffraction (XRD), respectively. The XRD measurements were carried out for all samples using parallel beam optics with a Cu $K\alpha$ radiation source with the scattering angle 2θ ranging from 30° to 55°. Figure 1(b) shows the obtained lattice parameters for all samples. The Fe_xCr_{100-x}, Fe and Co_xFe_{100-x} alloys show bcc (110) structures. With change of Co concentration (25% to 75%), they do not change crystal structure even though Co is expected to have an fcc (111) phase. Co, Ni, and CoNi alloys have fcc (111) structure. The FM layers such as Ni, Co, Co_xCu_{1-x}, and Co_xNi_{1-x} have fcc (111) structure when $Z > 27$, while Fe, Fe_xCr_{1-x}, and Co_xFe_{1-x} have bcc (110) structure for $Z < 27$. According to the report of Schoen *et al.* [18], the phase transition from fcc (111) to bcc (110) occurs at a specific concentration of 70% in the vicinity of Co.

B. Brillouin light scattering measurement

The physical quantities M_S, K_S, and D of our main interest are all determined by the BLS (Brillouin light scattering) technique [19]. In this study, a p-polarized laser with 300 mW of power with a 532 nm wavelength was used at the interfaces of the magnetic layer and the in-plane k vector is fixed at $k_x = 0.0167$ nm^{-1}, corresponding to the backscattered light by thermal excitation with an angle of incidence of 45°. From systematic BLS measurement, we obtained spin wave frequency dependent on the in-plane external magnetic field variations [11–13]. The typical field dependences of the resonance peaks are plotted in Fig. 2(a) for various thickness of $Pt/Co_{50}Fe_{50}$ layers (1.0–1.6 nm). From the resonance peaks, we can extract the effective anisotropy energy K_{eff} by using the following relation:

$$f = \frac{\gamma}{2\pi}\sqrt{H_{ex}(H_{ex} + H_{\text{eff}})}, \tag{1}$$

where $H_{\text{eff}} = \frac{2K_{\text{eff}}}{\mu_0 M_S}$ is the effective anisotropy field, and γ and μ_0 are the gyromagnetic ratio and vacuum permeability respectively.

Here, we ignore the bulk anisotropy contribution and consider only the interface perpendicular magnetic anisotropy. There are a small but nonzero contribution of the bulk anisotropy K_V, which causes underestimation of the M_S values, where the BLS measurements gave $M_{S,\text{BLS}} = \sqrt{M_S^2 - \frac{2K_V}{\mu_0}}$. We confirmed the discrepancies between $M_{S,\text{BLS}}$ and $M_{S,\text{VSM}}$, the saturation magnetization from VSM (vibrating sample magnetometer) measurement values (not shown here). The discrepancies are not substantial and the VSM measurements were carried out for thicker (20–30 nm) samples, while ultrathin 0.6–1.6 nm films were used for the BLS experiments. Therefore, the contributions of K_V are not significant in our study. Furthermore we assumed two anisotropies from two interfaces (Pt/FM and FM/MgO) are the same;

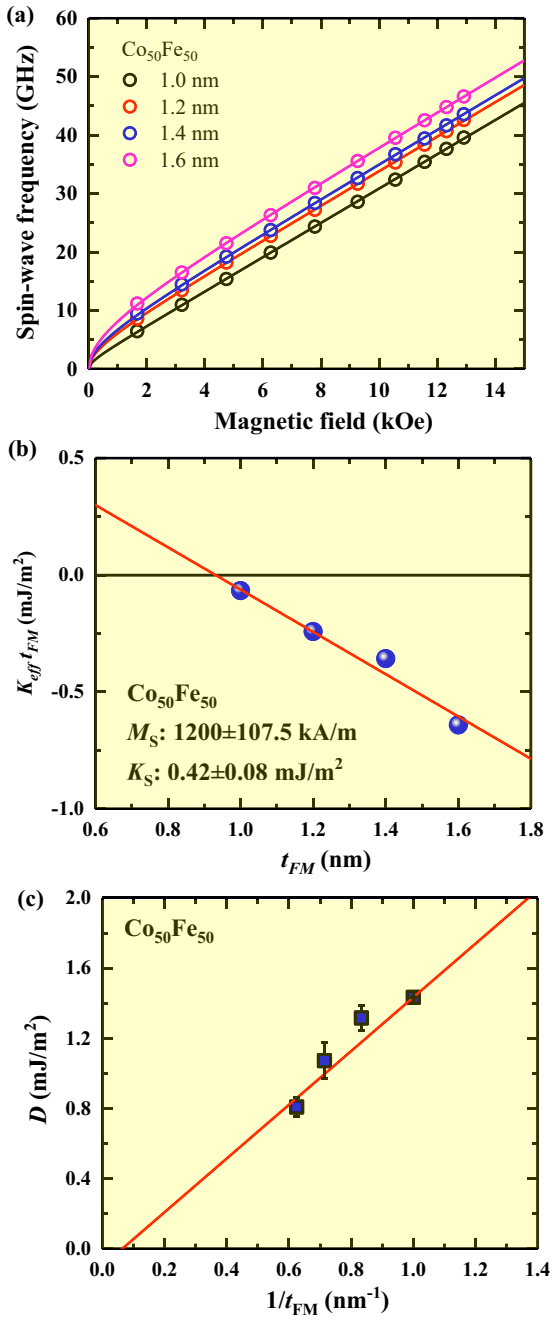

FIG. 2. (a) Typical spin wave resonance frequencies with fitting lines as a function of external in-plane magnetic field. (b) $K_{\rm eff}t_{\rm FM}$ vs $t_{\rm FM}$ plot of Pt/$Co_{50}Fe_{50}$ layers ($t_{\rm FM}$ = 1.0–1.6 nm). We can obtain M_S and $K_{\rm eff}$ from the slope and the intercept. (c) D is plotted against $t_{\rm FM}^{-1}$ with a linear fit. We repeated all measurement procedures for each composition sample.

we have $K_{\rm eff} = \frac{2K_S}{t_{\rm FM}} - \frac{1}{2}\mu_0 M_S^2$,

$$K_{\rm eff}t_{\rm FM} = 2K_S - \left(\tfrac{1}{2}\mu_0 M_S^2\right)t_{\rm FM}. \qquad (2)$$

We plotted $K_{\rm eff}t_{\rm FM}$ vs $t_{\rm FM}$ in the graph in Fig. 2(b) for Pt/$Co_{50}Fe_{50}$ layers. From the linear fitting using Eq. (2), we can obtain M_S and K_S for each composition sample from the slope and intercept, respectively. The iDMI energy density D is determined from the difference of the Stokes ($f_{\rm S}$) and anti-Stokes ($f_{\rm AS}$) resonance peak of $\Delta f = |f_{\rm S} - f_{\rm AS}| = \frac{2\gamma D}{\pi M_S}k_x$, where k_x is the propagating spin wave in-plane wave vector. Here, we used the absolute value of D; however, the signs of all D in the present study are the same as the Pt/Co/MgO. Usually, it is negative values, so all our series have negative D, when the Pt layer served as the bottom layer. The sign of D values has been deeply discussed in our previous work [20]. We assumed the same value of γ for all 3d FM alloys. The results are shown in Fig. 2(c) for Pt/$Co_{50}Fe_{50}$/MgO layers, and the linear proportionality to $t_{\rm FM}^{-1}$ is consistent with the interface origin of iDMI.

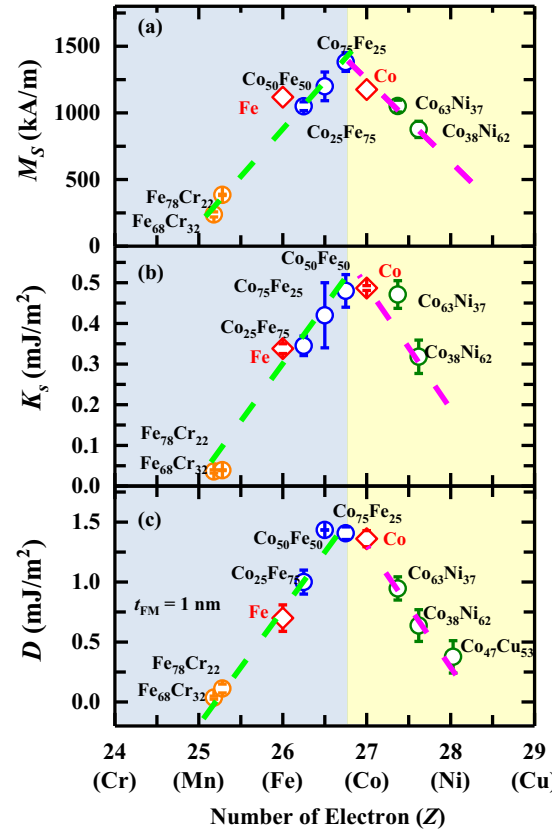

FIG. 3. Experimentally determined (a) M_S, (b) K_S, and (c) D from the BLS measurements of 0.6–1.6 nm thick FM layers. The M_S and K_S values are determined from the thickness-dependent effective anisotropy measurements. The D values are shown only for 1 nm thick FM samples. The green and magenta dashed lines are a guide for the eye.

C. Measured M_S, K_S, and D

The experimentally determined M_S, K_S, and D values are plotted as functions of Z in Figs. 3(a)–3(c). Figure 3(a) shows a typical SP-curve behavior (Λ shape) of M_S peaked at $Z \sim 26.5$; this behavior of the ultrathin film samples ($t_{\rm FM}$ = 0.6–1.6 nm) is very similar to the typical SP-curve behavior of bulk 3d FM alloys that is well explained by the Z-dependent band filling with the rigid band model [15–17]. Similar trends have been confirmed for relatively thicker (t = 2–10 nm) 3d FM alloys [18,21]. In addition to such ultrathin films, we carried out FMR (ferromagnetic resonance) experiments to determine the $M_{S,\rm FMR}$ values for the 20-nm series (see Sec. 1

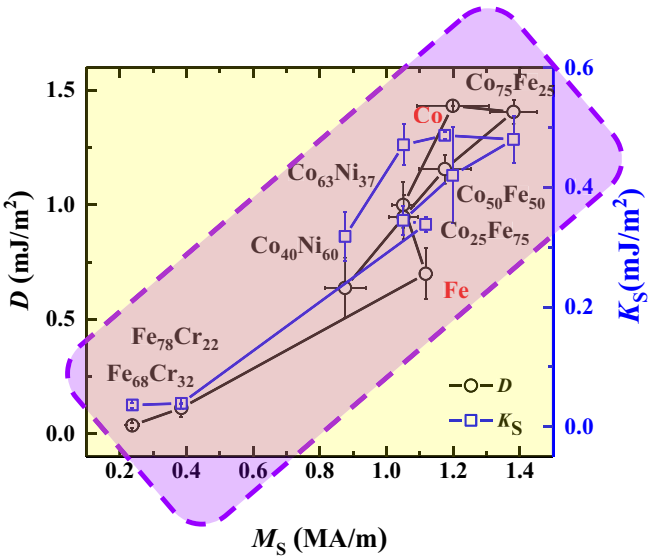

FIG. 4. Correlations among experimentally measured M_S, K_S, and D. They are somewhat scattered in detail; however, there are clear overall strong positive correlations. It clearly suggests that the three physical quantities (M_S, K_S, and D) have strong correlations in a wide range of electron numbers; however, the large scattering of the data implies that the correlation is only valid over a wide range variations.

of the Supplemental Material [22]). The SP-curve behavior of $M_{S,\mathrm{FMR}}$ for the 20-nm series is depicted in Fig. S2 [22]. The overall behavior of $M_{S,\mathrm{FMR}}$ is similar to the SP curve. However, there are some discrepancies: $M_{S,\mathrm{FMR}}$ is slightly larger than M_S from the BLS ($M_{S,\mathrm{BLS}}$) measurement. Since $M_{S,\mathrm{FMR}}$ is obtained with a thick FM layer (20 nm), while $M_{S,\mathrm{BLS}}$ is determined from thin layers ($\sim$1 nm), the small differences are acceptable. Another interesting point is that the maximum occurs at a different composition. While the bulk SP curve is maximal at Fe-rich composition, $M_{S,\mathrm{BLS}}$ takes a maximum at the Co-rich composition. In $M_{S,\mathrm{FMR}}$, the maximum is found around $Co_{50}Fe_{50}$, which is close to the bulk cases.

Figure 3(b) shows K_S values as a function of Z, which also shows a similar trend to the SP curve in M_S. The recent experiment by Schoen *et al.* [18] reported the similar behavior of K_S for ultrathin 3*d* transition metal binary alloys such as Ni-Co, Ni-Fe, and Co-Fe, which is attributed to the proportionality of the anisotropy energy and spin density at the interface.

Figure 3(c) shows D values as a function of Z for the 1 nm thick FM alloy layers. It also shows the SP-like behavior, increasing with Z and showing a maximum at $Z \approx 26.5$ ($Co_{50}Fe_{50}$), then decreasing with the further increase of Z. Thus D as a function of Z [Fig. 3(c)] exhibits very similar Z dependence as M_S does [Fig. 3(a)]. The peaks are at $Z \approx 26.5$ for both D and M_S.

A similar feature of three physical quantities (M_s, K_S, and D) on the Z dependence as shown in Figs. 3(a)–3(c) is the central point of the present study. Such similarity is well presented in Fig. 4, where M_S, K_S, and D are plotted altogether. The strong positive correlations among the three quantities are clearly seen. Here, however, it must be emphasized that the correlation is only valid over a wide range variations. There are many exceptional cases in the K_S and D values within the small variations because the K_S and D values depend on the fine structure of their bands and details of the interface hybridizations. However, at a large-scale variation of Z, the above-mentioned positive correlation emerges.

III. THEORETICAL CALCULATIONS

A. Rashba model calculation of *D*

In order to support the experimental results, we carried out theoretical model calculations in the framework of a two-dimensional (2D) tight-binding Hamiltonian with a Rashba interface. First of all, D and K_S require SOC, symmetry breaking, and exchange coupling as their core ingredients. As a simple toy model that captures all three core ingredients, we adopt a two-dimensional (2D) Rashba model [23]. M_S is calculated by a simple sum of the spin expectation value of the occupied states, and K_S of the model can be obtained from the total energy difference between perpendicular and in-plane magnetizations. Furthermore D can be calculated by considering position-dependent magnetization directions. By assuming the spatial variation is weak and treating it perturbatively, we have calculated D as a function of the band filling. The model consists of the majority and minority bands. The top and bottom of the majority band are shifted from those of the minority band, similar to the band diagram in Fig. 1(a). We calculate the iDMI part of the free energy F for the 2D Hamiltonian [22], Here, D is treated as a single constant as a first approximation. In general, D is tensor whose magnitude is proportional to SOC strength and the spatial derivative of magnetization [24,25],

$$\mathcal{H} = \epsilon_{\boldsymbol{k}} + \alpha_R(\boldsymbol{p} \times \hat{\boldsymbol{z}}) \cdot \boldsymbol{\sigma} + J_{sd}\boldsymbol{m} \cdot \boldsymbol{\sigma}, \tag{3}$$

where $\epsilon_{\boldsymbol{k}}$ is the kinetic energy, α_R is the Rashba constant, $\boldsymbol{p}$ is given by Eq. (11) below, $\hat{\boldsymbol{z}}$ is the unit vector along the inversion symmetry breaking axis, $\boldsymbol{\sigma}$ is the vector of the Pauli matrices, J_{sd} is the *sd* exchange strength, and $\boldsymbol{m}$ is the unit vector along the magnetization. To see the effects of DMI on magnons (cf. Refs. [24,25] for free energy), we consider a small variation $\delta\boldsymbol{m}$ from uniform magnetization $\boldsymbol{m}$. Using the perturbation theory, one obtains

$$F = \frac{1}{4}\alpha_R J_{sd}^2 \int d^2x \sum_{i=x,y}\sum_{\alpha=x,y} C_i^{\alpha}(\delta\boldsymbol{m} \times \partial_i \delta\boldsymbol{m})_{\alpha}, \tag{4}$$

The coefficients of the iDMI are given by

$$C_i^{\alpha} = \sum_{j=x,y} \epsilon_{\alpha j} A_{ij} + \epsilon_{\alpha i} B_i \quad (\alpha, i = x, y), \tag{5}$$

with

$$A_{ij} = \frac{1}{V}\sum_{\boldsymbol{k}} v_i^0 \frac{\hbar p_j(k_j)}{\Delta_{\boldsymbol{k}}^2}\Big[\delta(\mu - E_{\boldsymbol{k}}^+) + \delta(\mu - E_{\boldsymbol{k}}^-) + \frac{\Theta(\mu - E_{\boldsymbol{k}}^+) - \Theta(\mu - E_{\boldsymbol{k}}^-)}{\Delta_{\boldsymbol{k}}}\Big], \tag{6}$$

$$B_i = \frac{1}{V}\sum_{\boldsymbol{k}} \frac{p'(k_i)}{\Delta_{\boldsymbol{k}}}[\delta(\mu - E_{\boldsymbol{k}}^+) - \delta(\mu - E_{\boldsymbol{k}}^-)]. \tag{7}$$

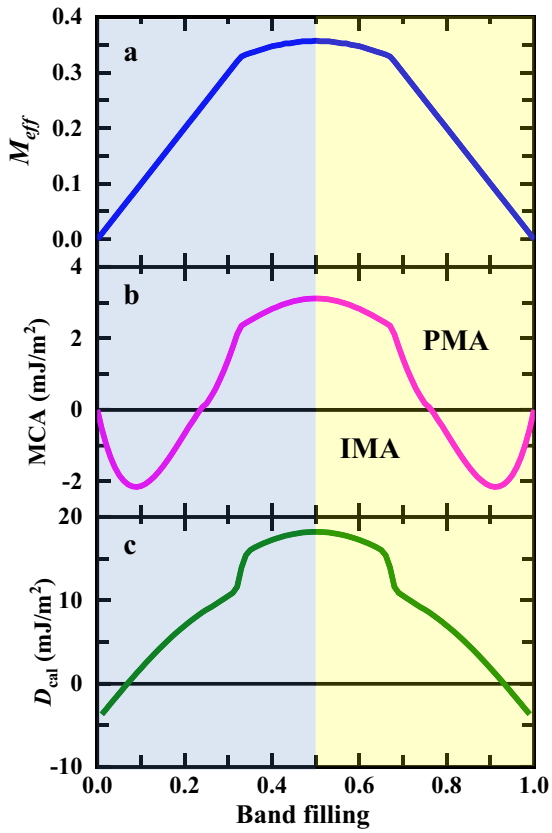

FIG. 5. (a) $\boldsymbol{M}$, (b) MCA, and (c) $D_{\rm calc}$ as a function of band filling calculated for the 2D Rashba model.

where $\epsilon_{xy} = -\epsilon_{yx} = 1$, $\epsilon_{xx} = \epsilon_{yy} = 0$, $V(=A_0 t_F)$ is the volume of the system, A_0 (t_F) is the area (thickness) of the system, $\delta(x)$ is the Dirac delta function, $\Theta(x)$ is the Heaviside step function where $\Theta(x > 0) = 1$ and $\Theta(x < 0) = 0$, μ is the chemical potential, and

$$E_{\boldsymbol{k}}^{\pm} = \epsilon_{\boldsymbol{k}} \pm \Delta_{\boldsymbol{k}}, \tag{8}$$

$$\Delta_{\boldsymbol{k}} = \sqrt{(J_{sd} m_x + \alpha_R p_y)^2 + (J_{sd} m_y - \alpha_R p_x)^2 + (J_{sd} m_z)^2}. \tag{9}$$

We assume a square lattice,

$$\epsilon_{\boldsymbol{k}} = -2t[\cos(k_x a) + \cos(k_y a)], \quad v_i^0 = \frac{2at}{\hbar} \sin(k_i a), \tag{10}$$

$$p_i(k_i) = \sin(k_i a)/a, \quad p_i'(k_i) = \cos(k_i a), \tag{11}$$

where t is the hopping parameter, and a is the lattice constant.

In Fig. 5(a), we calculate the magnetization M as a function of the band filling. Here, M is defined by

$$M \equiv \frac{n_{\rm up} - n_{\rm dn}}{n_{\rm max}}, \tag{12}$$

where $n_{\rm up(dn)}$ is the majority (minority) spin density for a given band filling, and $n_{\rm max}$ is the electron density for the maximum band filling. Thus, M is the normalized difference between majority and minority spin densities which is the definition of magnetization in 2D Rashba ferromagnetic system. The result shows that the magnetization follows the SP-curve behavior and our 2D Rashba tight-binding model successfully mimics the 3d transition metal ferromagnet.

We plotted MCA (magnetocrystalline anisotropy) energy in Fig. 5(b), which can be obtained in the same framework [22]. Note that K_S vanishes for the zero band filling (both majority and minority bands are empty) and 1 (both bands are completely filled), and takes a maximum at an intermediate filling. This is natural since the exchange coupling shifts the majority and the minority bands in opposite directions, and thus the net effect on the total energy becomes zero when the majority and minority bands are either both empty or both fully filled. Thus, the band filling dependence of K_S is qualitatively similar to the SP curve although the feature of the negative K_S for small and almost full band filling does not have counterparts in our experimental result.

In Fig. 5(c), we show the iDMI energy $D_{\rm calc} = (1/4)\alpha_R J_{sd}^2 (A_{xx} + B_x)$ as a function of the band filling. For numerical computation, we choose the lattice constant $a = 0.3$ nm, the area of the system $A = L \times L$ where $L = 60$ nm, the sd exchange strength $J_{sd} = 1.0$ eV, the Rashba parameter $\alpha_R = 0.5$ eV Å, and the hopping parameter $t = 0.4233$ eV. We align the unit vector $\boldsymbol{m}$ to $+\hat{\boldsymbol{z}}$ which is the direction of magnetization.

In contrast to M_S and K_S, D does not vanish at the band edges. This is due to the special feature of two-dimensional systems. Interestingly, D also exhibits a sign change at small band filling and close to full filling, which we attribute to the crossover into the parabolic dispersion regime. Although the model clearly has limitations quantitatively, we expect that, at the qualitative level, it is worth noting that this simple toy model reproduces the SP-like increase and decrease as a function of the band filling for M_S, K_S, and D.

B. First-principles calculations of K_S by virtual crystal approximation

For more quantitative analysis, the first-principles calculations are carried out using the full-potential linearized augmented plane wave (FLAPW) [26,27] method as implemented in FLEUR [28]. Alloys are treated using the virtual crystal approximation (VCA), where the number of valence electrons of alloys is weighted by the composition. Six atomic layers (hexalayer, corresponding to ∼0.9 nm thickness) of 3d ferromagnetic alloys on top of Pt (111) is considered, which is mainly discussed. For comparison, monolayer 3d FM alloys are also double checked, where M_S decreases monotonically with increasing Z in the range 26 (Fe) $< Z <$ 28 (Ni). Total magnetic moment, M_S, is shown in Fig. S3(a) [22] for the hexalayer case, which includes the induced moment of the Pt atom by the proximity effect. The Λ-shaped SP-like behavior is well reproduced with a peak at $Z \approx$ 26.5, in reasonable agreement with our experimental results [Fig. 3(a)].

K_S for a 3d FM alloy hexalayer is also calculated (Fig. S3(c) [22]); K_S also exhibits the Λ-shaped SP feature with maximum at $Z = 26.30$, which agrees with experiment [Fig. 3(b)]. The Λ shape in the range of $26.75 < Z < 27.5$ is not as smooth as M_S. However, the overall feature of

the Λ shape is well retained. As in the case of M_S, K_S by other calculations has different peak position. See Sec. 2 of the Supplemental Material for more details [22]; see, also, Refs. [7,14,26–37] therein.

C. Spin mixing conductance with surface Green's function method

In contrast to our experiment focusing on the band filling dependence of 3*d* FM, Ma *et al.* [38,39] examined the band filling effect of 5*d* HM in 3*d* FM/5*d* HM bilayers. They found that the 5*d* band filling affects the iDMI considerably. They also found a correlation between the iDMI and the spin mixing conductance (SMC), which is another important interfacial property that describes the spin transport through the interfaces. Zhu *et al.* [40] reported the linear relationship between K_S and D, and SMC scales approximately as the square of K_S at the Pt/FM interfaces.

In order to check the correlations between the iDMI and SMC [38–40], we examine the possible variation of the SMC with the band filling through a simple model calculation without realistic details. For this purpose, we employ a tight-binding Hamiltonian with the additional Rashba term at the interface between the FM and HM layers [41]. With the surface Green's function method, the SMC is calculated as a function of the band shift of the whole 3*d* bands relative to the 5*d* band (see Sec. 3 and Fig. S7 of the Supplemental Material [22] and Refs. [42–45] therein). Here, the band shift is equivalent to the band filling. As seen, SMC shares a similar trend with the SP curve. Since the SMC is defined in terms of the spin-dependent reflection and transmission matrices, the difference in the DOS of majority and minority bands at the Fermi level is important. Therefore, it should be of the SP-curve shape. It is easily understandable with the role of the relative band position of the Pt layer in the conductivity calculations as shown in Fig. S6 [22], in which schematics of the DOS of 3*d* transition metals (Fe, Co, and Ni) and Pt are depicted.

IV. CONCLUSION

In summary, we measured the three important interfacial magnetic properties M_S, K_S, and D, for 3*d* transition metal alloy ultra-thin layers on Pt heavy metal layer. By alloying 3*d* metals, we varied the number of electrons of FM layer over a wide range ($Z = 25$–28), and found that these three quantities exhibit the SP-curve like behavior. Although M_S is known as a bulk properties whereas K_S and D by purely interface properties, they showed strong positive correlations. We explained the SP-like behavior with a band filling model not only for M_S, but also for K_S and D. We conclude that M_S, K_S, and D in FM/HM bilayers are closely correlated over a wide range of electrons number variations.

ACKNOWLEDGMENTS

C.-Y.Y. is supported by the National Research Foundation of Korea (Grants No. 2020M3F3A2A02082437, No. 2021R1A2C2007672, and No. 2021M3F3A2A01037525), H.-W.L. is supported by the NRF (Grant No. 2018R1A5A6075964), K.-J.L. is supported by the NRF (Grant No. 2020R1A2C3013302), S.S.H.R. is supported by the NRF (Grant No. 2019R1I1A3A01059880), and H.K. is supported by JSPS KAKENHI (Grants No. JP21H01799, No. JP17H02929, No. JP19K03744).

C.-Y.Y. and N.-H.K. conceived the original idea. C.-Y.Y. and N.-H.K. planned and designed the experiments. N.-H.K. fabricated the samples. N.-H.K. measured all experimental data with E.B and J.-S.K. and analyzed data under the supervision of C.-Y.Y. Q.u.A. and S.S.H.R. performed first-principles calculations. H.-J.P., H.K., and K.-J.L. calculated 2D Rashba calculations. H.-W.L. and C.-Y.Y. calculated spin mixing conductance. N.-H.K. wrote the paper with S.S.H.R., H.-W.L., and C.-Y.Y. All the authors discussed the results and commented on the paper.

The authors declare no competing interests.

N.-H.K. and Q.u.A contributed equally to this work.

[1] J. Sampaio, V. Cros, S. Rohart, A. Thiaville, and A. Fert, Nat. Nanotechnol. **8**, 839 (2013).

[2] S. Ikeda, K. Miura, H. Yamamoto, K. Mizunuma, H. D. Gan, M. Endo, S. Kanai, J. Hayakawa, F. Matsukura, and H. Ohno, Nat. Mater. **9**, 721 (2010).

[3] L. Liu, O. J. Lee, T. J. Gudmundsen, D. C. Ralph, and R. A. Buhrman, Phys. Rev. Lett. **109**, 096602 (2012).

[4] A. Fert, V. Cros, and J. Sampaio, Nat. Nanotechnol. **8**, 152 (2013).

[5] C.-Y. You, Nat. Electron. **2**, 176 (2019).

[6] F. Hellman, A. Hoffmann, Y. Tserkovnyak, G. S. D. Beach, E. E. Fullerton, C. Leighton, A. H. MacDonald, D. C. Ralph, D. A. Arena, H. A. Dürr, P. Fischer, J. Grollier, J. P. Heremans, T. Jungwirth, A. V. Kimel, B. Koopmans, I. N. Krivorotov, S. J. May, A. K. Petford-Long, J. M. Rondinelli *et al.*, Rev. Mov. Phys. **89**, 025006 (2017).

[7] P. Bruno, Phys. Rev. B **39**, 865 (1989).

[8] H. Jia, B. Zimmermann, and S. Blügel, Phys. Rev. B **98**, 144427 (2018).

[9] S. Kim, K. Ueda, G. Go, P.-H. Jang, K.-J. Lee, A. Belabbes, A. Manchon, M. Suzuki, Y. Kotani, T. Nakamura, K. Nakamura, T. Koyama, D. Chiba, K. T. Yamada, D.-H. Kim, T. Moriyama, K.-J. Kim, and T. Ono, Nat. Commun. **9**, 1648 (2018).

[10] L. Zhu, K. Sobotkiewich, X. Ma, X. Li, D. C. Ralph, and R. A. Buhrman, Adv. Funct. Mater. **29**, 1805822 (2019).

[11] N.-H. Kim, D.-S. Han, J. Jung, K. Park, H. J. M. Swagten, J.-S. Kim, and C.-Y. You, Appl. Phys. Express **10**, 103003 (2017).

[12] J. Cho, N.-H. Kim, J. Jung, D.-S. Han, H. J. M. Swagten, J.-S. Kim, and C.-Y. You, IEEE Trans. Magn. **54**, 1500104 (2018).

[13] W.-Y. Kim, H. K. Gweon, K.-J. Lee, and C.-Y. You, Appl. Phys. Express **12**, 053007 (2019).

[14] A. Belabbes, G. Bihlmayer, F. Bechstedt, S. Blugel, and A. Manchon, Phys. Rev. Lett. **117**, 247202 (2016).

[15] L. Pauling, Phys. Rev. **54**, 899 (1938).

[16] J. Slater, J. Appl. Phys. **8**, 385 (1937).

[17] R. O'Handley, *Modern Magnetic Materials, Principles and Applications* (John Wiley & Sons, Inc., New York, 1999).
[18] M. A. W. Schoen, J. Lucassen, H. T. Nembach, T. J. Silva, B. Koopmans, C. H. Back, and J. M. Shaw, Phys. Rev. B **95**, 134410 (2017).
[19] J. Cho, N.-H. Kim, S. Lee, J.-S. Kim, R. Lavrijsen, A. Solignac, Y. Yin, D.-S. Han, N. J. J. van Hoof, H. J. M. Swagten, B. Koopmans, and C.-Y. You, Nat. Commun. **6**, 7635 (2015).
[20] J. Cho, N.-H. Kim, S. K. Kang, H.-K. Hwang, J. Jung, H. J. M. Swagmen, J.-S. Kim, and C.-Y. You, J. Phys. D: Appl. Phys. **50**, 425004 (2017).
[21] M. A. W. Schoen, J. Lucassen, H. T. Nembach, B. Koopmans, T. J. Silva, C. H. Back, and J. M. Shaw, Phys. Rev. B **95**, 134411 (2017).
[22] See Supplemental Material at http://link.aps.org/supplemental/10.1103/PhysRevB.105.064403 for details about determination of MS by ferromagnetic resonance experiments, Rashba model calculations of D, calculations of KS by virtual crystal approximation, and calculations of spin mixing conductance by the surface Green's function method.
[23] K. W. Kim, K. J. Lee, H. W. Lee, and M. D. Stiles, Phys. Rev. B **94**, 184402 (2016).
[24] I. A. Ado, A. Qaiumzadeh, A. Brataas, and M. Titov, Phys. Rev. B **101**, 161403(R) (2020).
[25] I. A. Ado, A. Qaiumzadeh, R. A. Duine, A. Brataas, and M. Titov, Phys. Rev. Lett. **121**, 086802 (2018).
[26] E. Wimmer, H. Krakauer, M. Weinert, and A. J. Freeman, Phys. Rev. B **24**, 864 (1981).
[27] M. Weinert, G. Schneider, R. Podloucky, and J. Redinger, J. Phys.: Condens. Matter **21**, 084201 (2009).
[28] FLEUR Project, available at: http://www.flapw.de.
[29] J. M. Schoen and S. P. Denker, Phys. Rev. **184**, 864 (1969).
[30] G. Moulas, A. Lehnert, S. Rusponi, J. Zabloudil, C. Etz, S. Ouazi, M. Etzkorn, P. Bencok, P. Gambardella, P. Weinberger, and H. Brune, Phys. Rev. B **78**, 214424 (2008).
[31] H. X. Yang, M. Chshiev, B. Dieny, J. H. Lee, A. Manchon, and K. H. Shin, Phys. Rev. B **84**, 054401 (2011).
[32] T. Maruyama, Y. Shiota, T. Nozaki, K. Ohta, N. Toda, M. Mizuguchi, A. A. Tulapurkar, T. Shinjo, M. Shiraishi, S. Mizukami, Y. Ando, and Y. Suzuki, Nat. Nanotechnol. **4**, 158 (2009).
[33] S.-S. Ha, N.-H. Kim, S. Lee, C.-Y. You, Y. Shiota, T. Maruyama, T. Nozaki, and Y. Suzuki, Appl. Phys. Lett. **96**, 142512 (2010).
[34] J. P. Perdew, J. A. Chevary, S. H. Vosko, K. A. Jackson, M. R. Pederson, D. J. Singh, and C. Fiolhais, Phys. Rev. B **46**, 6671 (1992).
[35] G. G. Kurdjumov and G. Sachs, Z. Phys. **64**, 325 (1930).
[36] D. T. Dekadjevi, B. J. Hickey, S. Brown, T. P. A. Hase, B. D. Fulthorpe, and B. K. Tanner, Phys. Rev. B **71**, 054108 (2005).
[37] J. Shen, P. Ohresser, Ch. V. Mohan, M. Klaua, J. Barthel, and J. Kirschner, Phys. Rev. Lett. **80**, 1980 (1998).
[38] X. Ma, G. Yu, C. Tang, X. Li, C. He, J. Shi, K. L. Wang, and X. Li, Phys. Rev. Lett. **120**, 157204 (2018).
[39] X. Ma, G. Yu, S. A. Razavi, L. Chang, L. Deng, Z. Chu, C. He, K. L. Wang, and X. Li, Phys. Rev. B **98**, 104428 (2018).
[40] L. Zhu, D. C. Ralph, and R. A. Buhrman, Phys. Rev. Lett. **123**, 057203 (2019).
[41] C. Barreteau, D. Spanjaard, and D. Desjonquères, C. R. Phys. **17**, 406 (2016).
[42] Y. Tserkovnyak, A. Brataas, and G. E. W. Bauer, Phys. Rev. Lett. **88**, 117601 (2002).
[43] M. Zwierzycki, Y. Tserkovnyak, P. J. Kelly, A. Brataas, and G. E. W. Bauer, Phys. Rev. B **71**, 064420 (2005).
[44] J. Mathon, Phys. Rev. B **56**, 11810 (1997).
[45] J. Mathon, A. Umerski, and M. Villeret, Phys. Rev. B **55**, 14378 (1997).